A two-dimensional correlation spectroscopic analysis on the interaction between humic acids and TiO2 nanopaticles

DATASET · JANUARY 2015

READS
57

4 AUTHORS, INCLUDING:

Wei Chen
University of Science and Technology of China
9 PUBLICATIONS **27** CITATIONS
SEE PROFILE

Han-Qing Yu
University of Science and Technology of China
508 PUBLICATIONS **11,014** CITATIONS
SEE PROFILE

Environmental Science & Technology

Article

pubs.acs.org/est

Two-Dimensional Correlation Spectroscopic Analysis on the Interaction between Humic Acids and TiO_2 Nanoparticles

Wei Chen, Chen Qian, Xiao-Yang Liu, and Han-Qing Yu*

Department of Chemistry, University of Science and Technology of China, Hefei, Anhui 230026, China

Supporting Information

ABSTRACT: The elucidation of the interaction between TiO_2 nanoparticles (NPs) and natural organic matter (NOM) can help one to better understand the fates, features, and environmental impacts of NPs. In this work, two-dimensional (2D) Fourier transformation infrared (FTIR) correlation spectroscopy (CoS) assisted by the fluorescence excitation−emission matrix (EEM) method is used to explore the interaction mechanism of humic acid (HA) with TiO_2 NPs at a molecular level. The results show that the C═O bonds (carboxylate, amide, quinone, or ketone) and C−O bonds (phenol, aliphatic C−OH, and polysaccharide) of HA play important roles in their interaction with TiO_2 NPs. The adsorption process of HA onto the surface of TiO_2 NPs is different from the bonding process of the two species in solution. The forms of the relevant groups of HA and their consequent reaction with TiO_2 NPs are affected to a great extent by the solution pH and the surface charge of NPs. The 2D-FTIR-CoS method is found to be able to construct a comprehensive picture about the NOM-TiO_2 NPs interaction process. This 2D-FTIR-CoS approach might also be used to probe other complicated interaction processes in natural and engineered environments.

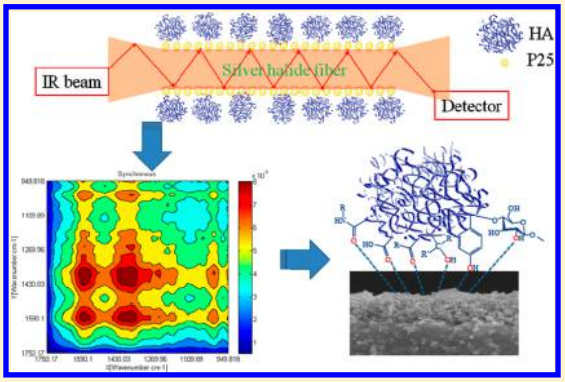

INTRODUCTION

Nanomaterials are part of human's daily life today, and manufactured nanoparticle (NP) products are being used for multiple applications.[1−3] Among them, TiO_2 NPs have been used as an environmentally friendly additive and photocatalyst in many areas, due to their extraordinary properties including high surface area and photosensitivity, strong catalytic and antimicrobial activity, and superior deodorizing and antifouling performance.[4,5] Specially, TiO_2 NPs are promising materials for water splitting and environmental remediation, owing to their highly efficient photocatalytic ability.[3,6] In aquatic systems, the ubiquitous presence of natural organic matter (NOM) strongly affects the morphology, performance, transformation, and potential environmental toxicity of various NPs like TiO_2 NPs.[7−9] Thus, elucidation of the interactions between TiO_2 NPs and NOM could be useful to a better understanding about their fate, feature, and environmental impact in aquatic environments.

NOM is an integrated term of organic compounds formed in the decomposition of plants and animal residues and during microbial metabolism and contains carboxyl, phenol, quinonyl, ester, ketone, hydroxyl, amino, and other functional groups.[10] The influence of NOM on the stability and photocatalytic ability of TiO_2 NP has been studied extensively.[7,11−14] However, little is known about the bonding mechanism between NOM and TiO_2 at a molecular level. Fluorescence excitation−emission matrix (EEM) spectroscopy combined with parallel factor (PARAFAC) analysis has been used for studying the complexes between NOM and metal or metallic compounds,[15−19] but this approach is not able to characterize the bonding features of nonfluorescent substances in NOM.

Fourier transform infrared (FTIR) spectroscopy offers a comprehensive insight into the molecular structure of principle organics in NOM, both fluorescent and nonfluorescent.[20,21] Thus, it is possible to explore the interaction between NOM and TiO_2 NPs by monitoring the FTIR spectra variation. Two-dimensional (2D) FTIR correlation spectroscopy (CoS), which analyzes a set of spectral data from a system under an external perturbation (e.g., time, temperature, concentration, etc.), greatly enhances the spectral resolution compared to the conventional FTIR spectra with overlapped peaks.[22−24] Furthermore, the relative directions and sequential orders of band intensity changes, i.e., structural variations, can be probed by the synchronous and asynchronous spectra of 2D-CoS.[24,25] 2D-CoS has become a popular and versatile tool to explore the combination and adsorption processes of metals and minerals.[26−28] To the best of our knowledge, 2D-FTIR-CoS has not been used to investigate the interactions between NOM and NPs.

Therefore, this work aimed to probe the bonding mechanism of NOM with NPs and the sequential order of corresponding

Received: May 22, 2014
Revised: July 24, 2014
Accepted: September 15, 2014
Published: September 15, 2014

   dx.doi.org/10.1021/es502502n | Environ. Sci. Technol. 2014, 48, 11119−11126

functional groups of humic acid (HA) adsorbed onto NPs at a molecular level. For these purposes, HA was used as a representative model of NOM, and the structural changes of HA as a function of pH and TiO_2 NP concentration were examined using FTIR spectroscopy coupled with 2D-CoS and EEM-PARAFAC analysis. In addition, the sorption spectra of HA on TiO_2 NP as a function of time were collected and analyzed by ATR-FTIR 2D-CoS to clarify the interaction process.

EXPERIMENTAL SECTION

Sample Preparation. AR-grade NaOH and HCl were purchased from Sinopharm Chemical Reagent Co., China. The TiO_2 benchmark (Degussa P25) was used. Commercial HAs (Sigma-Aldrich Co., USA) were purified prior to use.[29] Briefly, original HA was dissolved in NaOH solution (pH = 13.0) and filtered, followed by acidification to pH = 1.0 with HCl and filtration; then, the final precipitates were washed extensively with 0.1 M HCl and finally freeze-dried.

The purified HAs were dissolved to a final concentration of 100 mg/L in solutions with various pHs (ranging from 2.0 to 10.0), which were adjusted with 1 M NaOH and 1 M HCl. After being left for 12 h to reach dissociation equilibrium, 25 mL of each solution with different pH was freeze-dried for the FTIR measurements. By dispersing 10 mg of P25 powder into 10 mL of purified water (Milli-Q, 18 MΩ cm) and sonicating for 5 min, a bulk solution containing 1 g/L P25 was prepared and used to generate different concentrations of P25 solutions. The z-average hydrodynamic diameter of the P25 suspension was measured to be 2090 nm by the Nanosized ZS instrument (Malvern Instruments Co., UK), suggesting the aggregation of P25 NP in solution. A series of solutions (pH 7.0) containing 25 mg/L HA and P25 with a concentration ranging from 0 to 50 mg/L was prepared and shaken for 12 h at 25 °C to ensure complexation equilibrium. Then, the solutions were analyzed by fluorescence EEM spectroscopy. Twenty mL of each solution was freeze-dried for further FTIR spectroscopy analysis.

Spectroscopic Measurements. The attenuated total reflection (ATR) spectra of the freeze-dried HA samples with various pH values were recorded on a ZnGe equipped ATR attachment of a Vertex 70 spectrometer (Bruker Co., Germany) with a deuterated triglycine sulfate detector. The bands between 4000 and 600 cm^{-1} were recorded, and 32 scans were averaged for each spectra with a spectral resolution of 4 cm^{-1}. A mixture of 100 mg of KBr (IR grade) and freeze-dried HA with P25 of varying concentrations was ground, homogenized, and pressed. The FTIR spectra were obtained with the same settings used in ATR measurements. P25 samples at different concentrations in the absence of HA were treated by the same procedure, and their FTIR spectra were recorded as the background spectra of the corresponding P25 samples at the same concentration in the presence of HA.

Fluorescence EEMs were measured on a LS55 fluorescence spectrophotometer (PerkinElmer Co., USA). Scanning emission (Em) spectra from 300 to 600 nm were obtained in 0.5 nm increments by varying the excitation (Ex) wavelength from 250 to 450 nm in 10 nm increments with a scan rate of 1200 nm/min. Both the excitation and emission slit band widths were set as 10 nm. The EEM spectra were obtained after deducting the Rayleigh and Raman scattering by a homemade Matlab program. The conditional stability constant K of P25 to HA was estimated by the Modified Stern−Volmer equation (see details in the Supporting Information). PARAFAC analysis is described in detail elsewhere.[30]

An integrated planar-cylinder fiber, consisting of a flat silver halide fiber segment (refractive index of the waveguide $n_1 = 2.2$, length 45 mm, thickness 130 μm) with fiberoptic extensions (length 15 mm, thickness 700 μm) at both ends, was used as the active transducer.[31] 200 μL of the 1 g/L P25 bulk suspension was dropped onto the flat silver halide fiber segment. and the solvent was evaporated after drying on a heater for 4 h at 35 °C. After rinsing with Milli-Q water, a stable P25 deposit with an estimated thickness of 0.6 μm firmly and evenly adhered to the silver halide fiber was obtained (Figure S1, Supporting Information). The coated fiber was then placed in a sealed cell with two ends exposed to the optical path and rinsed with Milli-Q water extensively before each test. A background spectrum consisting of the combined absorbance of the waveguide fiber, the P25 deposit, and H_2O was obtained by collecting 64 scans at a 4 cm^{-1} resolution with an external liquid-nitrogen cooled MCT detector. Adsorption of HA onto P25 was performed by injecting 2 mL of HA solution (100 mg/L, pH = 5.0, 7.0, or 9.0) to the cell, soaking the waveguide fiber completely, and simultaneously recording the absorbance in the 1700−1000 cm^{-1} spectra range every 10 min within 2 h.

Analysis of 2D-CoS. In this work, pH, TiO_2 NPs concentration, and contact time were used as external perturbations for the structural changes of HA, its complexation with TiO_2 NPs, and its adsorption process onto TiO_2 NPs, respectively. A set of pH- and time-dependent ATR-FTIR spectra were thus collected, respectively. Prior to 2D analysis, the ATR spectra were baseline-corrected and denoised by Savitzky-Golay Smoothing. The practical computation of 2D-CoS was performed as proposed by Noda and Ozaki.[24] All calculations were performed using Matlab R2010a (Mathworks Inc., USA).

The sequential order of intensity change between two bands at ν_1 and ν_2 could be obtained from the sign of synchronous correlation peak $\Phi(\nu_1, \nu_2)$ and asynchronous correlation peak $\Psi(\nu_1, \nu_2)$ under the well-established principles.[24,32,33] In brief, the change in the spectral intensity at ν_1 band occurs prior to that at ν_2 if $\Phi(\nu_1, \nu_2)$ and $\Psi(\nu_1, \nu_2)$ have the same sign, while the order is reversed if $\Phi(\nu_1, \nu_2)$ and $\Psi(\nu_1, \nu_2)$ have the opposite sign. The changes at ν_1 and ν_2 occur simultaneously if $\Psi(\nu_1, \nu_2)$ is zero.

RESULTS

Structural Profiles of HA as a Function of pH. The influence of pH on HA structure was examined, and the ATR spectra of HA as a function of pH are illustrated in Figure 1. The spectral variations were focused on in the 1750−950 cm^{-1} region, where the absorption changed drastically. It could be observed that the peaks in the one-dimensional ATR-FTIR spectra strongly overlapped. With an increase in pH value, their absorption intensity enlarged at different levels, indicating the dissociation of HA and thus exposure of more absorption groups. However, the spectroscopic observation was not sufficiently sensitive to reveal the dynamics of the structural transformation.

To further clarify the transformation sequence of each HA functional group with increasing pH value, 2D-CoS analysis was performed and the results are displayed in Figure 2 and Table 1. The synchronous maps (Figure 2a,c) exhibited five prominent autopeaks on the diagonal at 1640, 1560, 1515, 1380, and 1030 cm^{-1}, in accordance with those obtained from

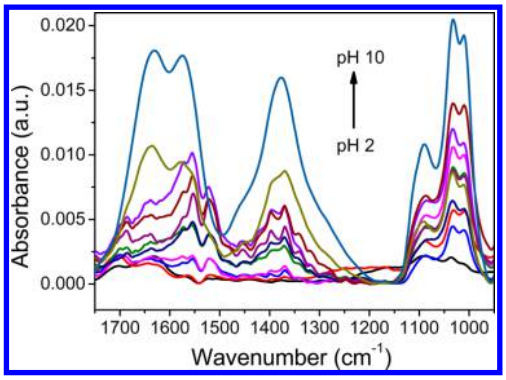

Figure 1. ATR-FTIR spectra of HA with the increasing pH from 2.0 to 10.0 in the region of 1750−950 cm^{-1}.

the second derivative spectra (Figure S2, Supporting Information). The change in band intensity followed the order 1030 > 1560 > 1640 > 1515, 1380 cm^{-1}. The assignments of these peaks are listed in Table 1. In addition, a small but not obvious autopeak at 1698 cm^{-1} was observed, attributed to the carboxylic acid C═O stretching vibration. The cross-peaks off the diagonal at 1640/1560, 1640/1515, 1640/1380, 1640/1030, 1560/1515, 1560/1380, 1560/1030, 1515/1380, 1515/1030, and 1380/1030 cm^{-1} all exhibited positive signs in the synchronous map, suggesting that these peaks originated from the same responses of spectral intensities to pH perturbation.

The 2D asynchronous spectra can help to judge the sequential order of specific events along external perturbations. The cross-peaks of every two bands are shown in the asynchronous maps (Figure 2b,d), and their signs are given in Table 1. In the asynchronous map, the red represents a positive sign, while the blue represents a negative sign. According to Noda's rule,[24] the sequence of band variation with pH follows the order 1640 → 1380 → 1560 → 1515, 1030 cm^{-1}. No cross-peak was observed at 1515 and 1030 cm^{-1}, indicating that these two bands changed simultaneously. Thus, as stimulated by increasing pH values, the structural changes of HA followed the order: C═O (amide, quinone, or ketones) > phenolic O−H > COO^- > aromatic C═C, polysaccharide C−O.

EEM and 2D-IR Analysis on the Interaction between HA and TiO_2 NPs. The EEM spectra of HA with the increasing P25 NPs concentration are shown in Figure 3. Three Peaks with Ex/Em centered at 250−270/380−420, 260−300/420−480, and 360−400/450−400 nm were identified. The PARAFAC modeling results in Figure S3, Supporting Information, show three independent components with Ex/Em located at 255/400 (C1), 280/450 (C2), and 380/470 (C3) nm, respectively. The fluorescence of C1 was located in the EEM region of P25, and its intensity increased with the increasing P25 concentration; thus, C1 was identified as P25 NPs. C2 and C3 could be attributed to carboxylic-like and phenolic-like fluorophores of HA, respectively.[18,34] With an increase in TiO_2 concentration, the fluorescence intensities of C1, C2, and C3 increased, decreased, and remained unchanged, respectively. Specially, the fluorescence intensity of C2 and C3 as a function of TiO_2 concentration is shown in Figure S4a, Supporting Information, and the conditional stability constant K of P25 NPs to C2 was calculated to be 0.0365 $(mg/L)^{-1}$

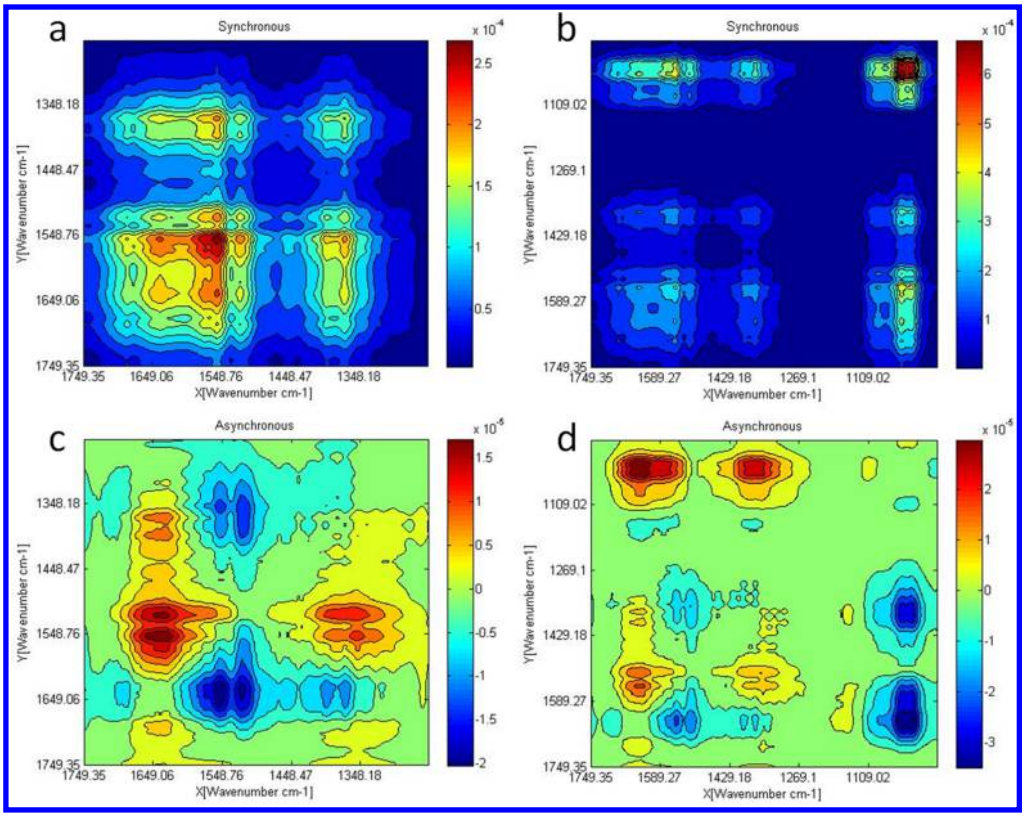

Figure 2. Synchronous (a, b) and asynchronous (c, d) 2D correlation maps generated from the 1750−1250 cm^{-1} region (a, c) and 1750−950 cm^{-1} region (b, d) of the ATR-FTIR spectra of HA with the increasing pH.

Table 1. 2D-CoS Results on the Assignment and Sign of Each Cross-Peak in Synchronous (Φ) and Asynchronous (Ψ, in the Brackets) Maps of HA with the Increasing pH[a]

		sign				
position (cm^{-1})	possible assignment	1640	1560	1515	1380	1030
1640	C═O stretching of amide, quinone, or H-bonded conjugated ketones, $\nu_{c=o}$	+	+(+)	+(+)	+(+)	+(+)
1560	COO^- symmetric stretching, $\nu_{coo\text{-}s}$		+	+(+)	+(−)	+(+)
1515	aromatic C═C stretching, $\nu_{c=c}$			+	+(−)	+(0)
1380	OH deformation, C−O stretching of phenolic OH or COO^- asymmetric stretching, $\nu_{coo\text{-}as}$				+	+(+)
1030	C−O stretching of polysaccharide or polysaccharide-like substances, $\nu_{c\text{-}o}$					+

[a]Signs were obtained in the upper-left corner of the maps.

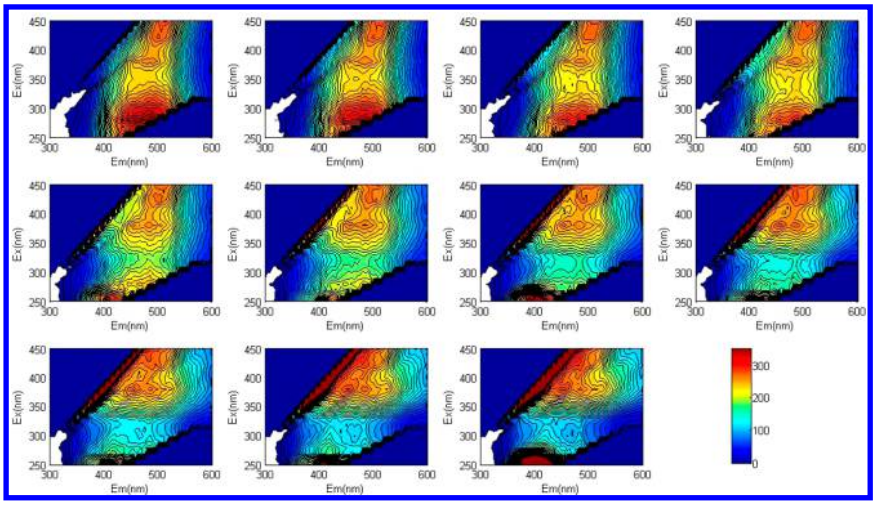

Figure 3. EEM matrix of HA (25 mg/L) with TiO_2 NPs at concentrations of 0, 1, 2.5, 5, 10, 15, 20, 25, 30, 40, and 50 mg/L at pH 7.0.

from the quenching curve (Figure S4b, Supporting Information).

Fluorescence quenching generally suggests a specific bonding of quencher to fluorophores.[35] The EEM-PARAFAC results indicate that the bonding of HA with P25 was associated with the carboxylic groups rather than the phenolic groups in HA. However, it is unknown whether there were interactions between P25 and the nonfluorescent groups of HA or not from the EEM-PARAFAC results alone.

Figure 4 shows the synchronous and asynchronous FTIR maps of HA with TiO_2 NP concentration as the perturbation. Four characteristic autopeaks at 1590, 1390, 1100, and 1030 cm^{-1} were observed in the synchronous spectra, and their intensity changed at the same direction based on the positive cross-peaks. The four bands were assigned to the symmetric stretching of COO^-, asymmetric stretching of COO^-, C−OH stretching of aliphatic OH, and C−O stretching of polysaccharides, respectively. The signs of the cross-peaks in the asynchronous spectra (Table S1, Supporting Information) suggest the sequential order of the bonding affinities of these bands with TiO_2 NPs is 1590, 1390 (COO^-) → 1100 (aliphatic C−OH) → 1030 (polysaccharides C−O) cm^{-1}. Thus, in addition to carboxyl groups, the C−O band of aliphatic C−OH and polysaccharides also contributed to the bonding of HA with TiO_2 NPs.

HA Adsorption onto TiO_2 NPs. To further clarify the interaction mechanism between HA and TiO_2 NPs, the adsorption of HA onto P25 as a function of time was spectroscopically analyzed. Since pH substantially affects the HA structure and then changes the adsorption process, three pH values (acidic pH 5.0, neutral pH 7.0, and alkaline pH 9.0) were selected. The ATR-FTIR spectra of HA on P25 at pH 7.0 as a function of time are presented in Figure S5a, Supporting Information. The striking spectral changes mainly occurred in the 1800−1000 cm^{-1} region, which exhibited main characteristic peaks of the adsorbed HA molecule. A successive increase in intensity upon HA sorption was observed with the increasing time. Five distinctive peaks, 1695, 1590, 1430, 1375, and 1020 cm^{-1}, were observed in the second derivative spectra (Figure S5b, Supporting Information). These observations indicate that HA could interact with P25 through multiple mechanisms because of its diverse functional moieties, which also exhibited the complexity and difficulty in the sorption process analysis.

2D-CoS was applied to examine the sorption functional groups of HA and their sequence in sorption onto P25. Figure 5a,b, respectively, shows the synchronous and asynchronous maps generated from the ATR-FTIR spectra at pH 7.0. Three main autopeaks (1590, 1410, and 1015 cm^{-1}) were displayed in the synchronous spectra, and their cross-peaks all exhibited positive signs, suggesting the same direction of these band intensity changes. In the asynchronous map, the band centered at 1410 cm^{-1} was divided into two bands at 1430 and 1380 cm^{-1}, and a series of cross-peaks correlated to 1680 cm^{-1} was observed, which was likely to be overlapped by the band at 1590 cm^{-1} in the synchronous spectra. The bands were attributed as follows: the band at 1680 cm^{-1} was assigned to the C═O stretching of amide, quinone, or ketone (trace), the band at 1590 and 1430 cm^{-1} to COO^- symmetric and antisymmetric stretching, the band at 1380 cm^{-1} to C−O stretching of phenol OH, and the band at 1015 cm^{-1} to C−O stretching of polysaccharides. The signs of cross-peaks in the asynchronous spectra (Table S2, Supporting Information)

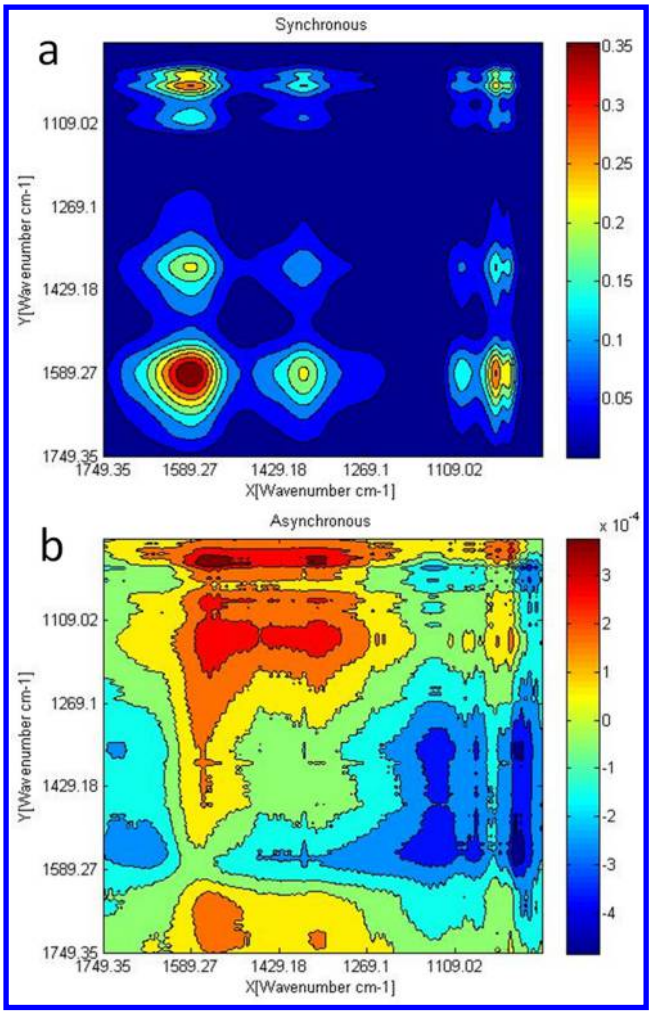

Figure 4. Synchronous (a) and asynchronous (b) 2D spectra in the 1750−950 cm^{-1} region generated from the FTIR spectra of HA with TiO_2 NP concentration as the perturbation.

indicate that the sequence of the sorption affinities of HA bands to TiO_2 NPs follows the order 1590, 1430 → 1015 → 1380 → 1680 cm^{-1}, demonstrating that the rank for the bonding of functional groups in HA with TiO_2 NPs is carboxylate C═O > polysaccharide C−O > phenol C−O > amide, quinone, or ketone C═O.

The adsorption of HA onto TiO_2 NPs under acidic (pH 5.0) and alkaline (pH 9.0) conditions was also investigated, and the synchronous/asynchronous spectra are shown in Figure 5c,d and Figure 5e,f, respectively. At pH 5.0, autopeaks were observed at 1560, 1398, and 1085 cm^{-1} in the synchronous spectra, corresponding to COO^-, phenol C−O, and polysaccharide C−O, respectively. Two other bands at 1706 and 1650 cm^{-1}, which overlapped in the synchronous spectra, could be identified from the cross-peaks in the asynchronous spectra. The band at 1706 cm^{-1} was assigned to the carboxylic acid C═O stretching vibration, and the band at 1650 cm^{-1} to amide, quinone, or ketone C═O. A band around 1510 cm^{-1} close to 1560 cm^{-1} appeared in the synchronous spectra, but not in the asynchronous spectra, attributed to the N−H of amide II. The signs of the 2D-CoS (Table S3, Supporting Information) suggest that these bands changed in the same direction and the sequential order was 1706 (carboxylic acid C═O) → 1650 (amide, quinone, or ketone C═O) → 1560 (carboxylate C═O) → 1398 (phenol C−O) cm^{-1}. At pH 9.0, the four main autopeaks centered at 1646, 1560, 1450, and 1360 cm^{-1} in the synchronous map corresponded to the shift of bands at 1680, 1590, 1430, 1380 cm^{-1} at pH 7.0, respectively. The band responsible for polysaccharide C−O was no longer observable, and a new autopeak at 1168 cm^{-1} was attributed to the C−OH stretching of aliphatic OH. A band at 1510 cm^{-1} also appeared. According to the signs of the 2D-CoS (Table S4, Supporting Information), these bands also changed in the same direction and their order followed 1360 → 1168 → 1560, 1450 → 1646 cm^{-1}. Thus, the bonding sequence to TiO_2 NPs at pH 9.0 was: phenol C−O > aliphatic C−OH > carboxyl C═O > amide, quinone, or ketone C═O.

DISCUSSION

The presence of NOM has shown a significant impact on the aggregation, disaggregation, and stabilization of TiO_2 NPs, as demonstrated by the dynamic light scattering and electrophoretic experiments.[11,12,14] However, robust evidence is needed to elucidate the interactions between NOM and TiO_2 NPs in detail. In this work, a 2D-FTIR-CoS method, assisted by fluorescence EEM, is successfully applied to explore the interaction mechanism between HA and TiO_2 NPs at a molecular level. This approach provides useful information about the dynamic process of bonding pathways of HA with TiO_2 NPs.

The EEM-PARAFAC analysis shows two primary components of HA with Ex/Em centered at 280/450 and 380/470 nm, corresponding to the carboxylic and phenolic groups of HA. Under neutral conditions, change of their intensity with the increasing P25 concentration indicates that the bonding of HA with P25 is associated with carboxylic groups, rather than phenolic groups in HA. The 2D-FTIR-CoS results about the impact of the nonfluorescent component in HA on its bonding with TiO_2 NP show that, in addition to the carboxyl groups, the C−O band of aliphatic C−OH and polysaccharides also contribute to the bonding of HA with TiO_2 NPs. Besides, the asynchronous map of 2D-CoS gives the sequential order of these bands bonded to TiO_2 NPs: COO^- > aliphatic C−OH > polysaccharides C−O.

The 2D-ATR-FTIR-CoS analysis on the HA adsorption onto TiO_2 NPs shows some differences at different pH values. The structure of HA is highly dependent upon pH. HA is aggregated to form macromolecules, and the organic groups are trapped inside at a low pH.[36] An increase in pH causes the breaking of hydrogen bonds that hold HA molecules in the solid phase and increases the electrostatic repulsion among the negatively charged HA molecules that overcome the attractive intermolecular forces among individual HA particles.[37] As a result, a progressive dissolution occurs, and accordingly, the related functional groups become exposed. The charge on the TiO_2 NP surface changes from positive to negative with the increasing pH and is positively charged at pH ≤ 7.0.[14] In the acidic region, due to the aggregation of HA, only a small amount of functional groups (mostly carboxyl acid, trace COO^-, phenol, and amide, quinone, or ketone) are exposed and adsorbed to the NP surface. In the neutral region, HA aggregates begin to be dissociated and negatively charged, and carboxylate COO^- groups interact with NPs largely as oppositely charged patches. The bands change most significantly in this pH region. Some groups like polysaccharides C−O are released from the aggregates and adsorbed to the NP surface too. Both HA and TiO_2 NPs are negatively charged in

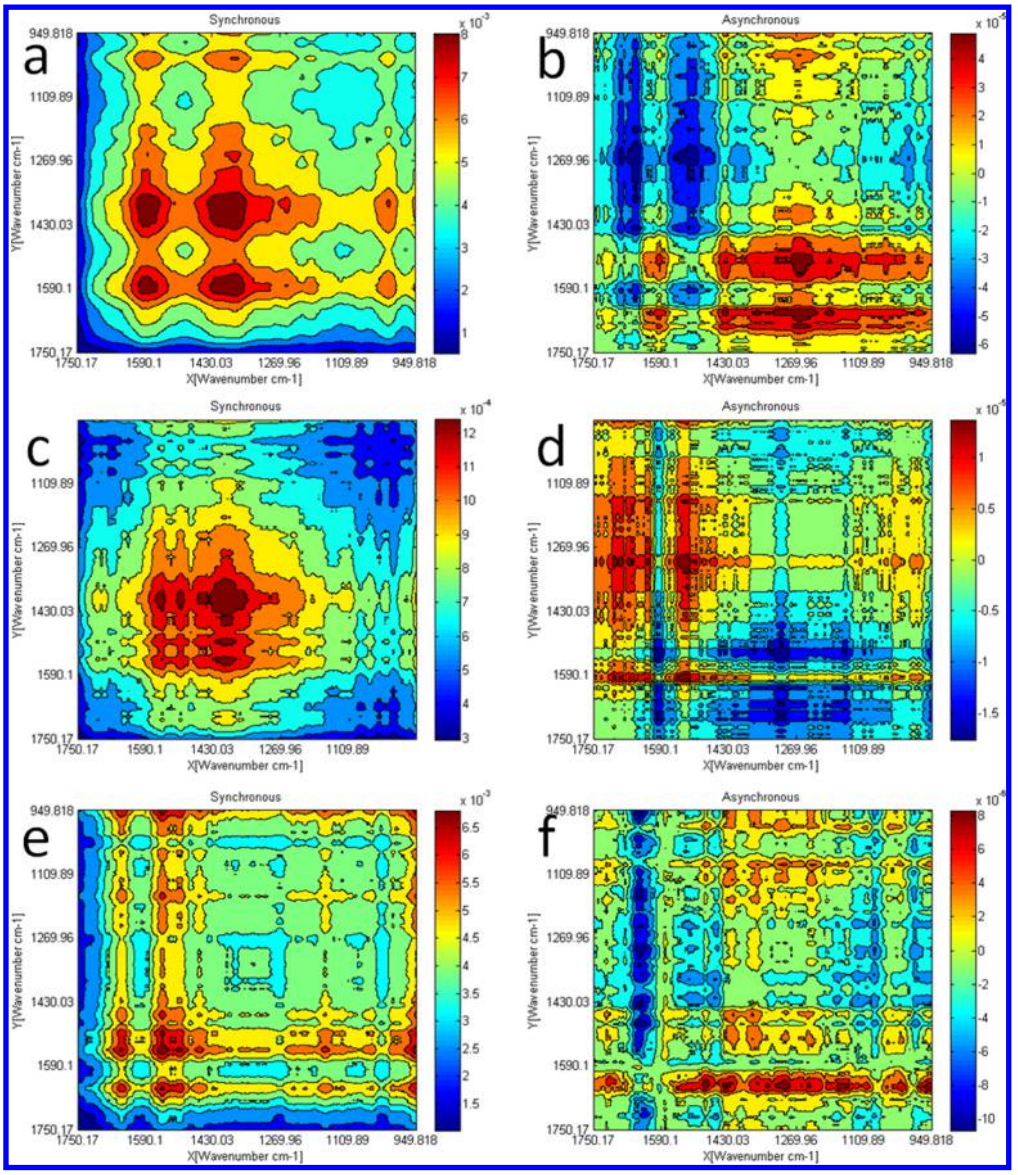

Figure 5. Synchronous (a, pH 7.0; c, pH 5.0; e, pH 9.0) and asynchronous (b, pH 7.0; d, pH 5.0; f, pH 9.0) 2D correlation spectra of HA adsorbed on P25 in the region of 1750−950 cm^{-1}.

the alkaline region, and the adsorption is suppressed because of the electrostatic repulsion. Besides, more free groups of HA including aliphatic C−OH are present in the solution and interact with NPs, owing to their further dissociation under alkaline conditions. As a result, the adsorption process of HA onto the surface of TiO_2 NP is somewhat different from the bonding process of these two species in solution. The forms of the relevant groups of HA and their consequent reaction with TiO_2 NPs are governed by the pH and the surface charge of TiO_2 NPs.

Although large amounts of TiO_2 NP products are being discharged into the environment, the mechanism for the interaction between TiO_2 NPs and NOM, the most abundant species in the aquatic environment, is not completely understood yet. In this work, we find that the C═O bonds of carboxylate, amide, quinone, or ketone groups and the C−O bonds of phenol, aliphatic C−OH, and polysaccharide groups of HA play important roles in its bonding and adsorption with TiO_2 NPs. The 2D-FTIR-CoS method assisted by the EEM-PARAFAC approach can help to construct a comprehensive picture of the NOM-NPs interacting process at a molecular level. Knowledge on the interaction capacity of NPs to different chemical groups of NOM and factors that influence the sequence of these interactions will help to better understand the status and transformation process of NPs in different aquatic systems, which subsequently govern the final fates of NPs in natural and engineered environments. Besides, the elucidation of NOM-NPs interactions is helpful for the design of new NPs which can work effectively in the presence of NOM in water and wastewater treatment. Furthermore, this 2D-FTIR-CoS approach may also find its application to other complicated interaction processes in natural and engineered environments.

■ ASSOCIATED CONTENT

Supporting Information

Detailed description about the calculation of conditional stability constant K; signs of cross-peaks in the 2D-CoS synchronous and asynchronous maps (Tables S1−S4); scanning electron microscopy image of P25 deposition on the

waveguide substrate (Figure S1); second derivative ATR-FTIR spectra of HA with the increasing pH (Figure S2); EEM-PARAFAC results of the three components (Figure S3); fluorescence intensity at Ex/Em = 280/450 nm and 380/470 nm as a function of TiO_2 concentration and Modified Stern−Volmer plot for the quenching of HA by TiO_2 at Ex/Em = 280/450 nm (Figure S4); ATR-FTIR spectra and second derivative spectra of HA on P25 with the increasing sorption time at pH 7.0 in the region of 1800−1000 cm^{-1} (Figure S5). This material is available free of charge via the Internet at http://pubs.acs.org/.

AUTHOR INFORMATION

Corresponding Author

*Fax: +86 551 63601592; e-mail: hqyu@ustc.edu.cn.

Notes

The authors declare no competing financial interest.

ACKNOWLEDGMENTS

We thank the Natural Science Foundation of China (51129803), Hefei Center for Physical Science and Technology (2012FXZY005), and the Program for Changjiang Scholars and Innovative Research Team in University of the Ministry of Education of China for the support of this study.

REFERENCES

(1) Roco, M. The long view of nanotechnology development: The national nanotechnology initiative at 10 years. *J. Nanopart. Res.* **2011**, *13* (2), 427−445.

(2) Auffan, M.; Rose, J.; Bottero, J.-Y.; Lowry, G. V.; Jolivet, J.-P.; Wiesner, M. R. Towards a definition of inorganic nanoparticles from an environmental, health and safety perspective. *Nat. Nanotechnol.* **2009**, *4* (10), 634−641.

(3) Qu, X.; Brame, J.; Li, Q.; Alvarez, P. J. J. Nanotechnology for a safe and sustainable water supply: Enabling integrated water treatment and reuse. *Acc. Chem. Res.* **2012**, *46* (3), 834−843.

(4) Weir, A.; Westerhoff, P.; Fabricius, L.; Hristovski, K.; von Goetz, N. Titanium dioxide nanoparticles in food and personal care products. *Environ. Sci. Technol.* **2012**, *46* (4), 2242−2250.

(5) Chen, X.; Mao, S. S. Titanium dioxide nanomaterials: Synthesis, properties, modifications, and applications. *Chem. Rev.* **2007**, *107* (7), 2891−2959.

(6) Theron, J.; Walker, J. A.; Cloete, T. E. Nanotechnology and water treatment: Applications and emerging opportunities. *Crit. Rev. Microbiol.* **2008**, *34* (1), 43−69.

(7) Uyguner-Demirel, C. S.; Bekbolet, M. Significance of analytical parameters for the understanding of natural organic matter in relation to photocatalytic oxidation. *Chemosphere* **2011**, *84* (8), 1009−1031.

(8) Wiesner, M. R.; Lowry, G. V.; Alvarez, P.; Dionysiou, D.; Biswas, P. Assessing the risks of manufactured nanomaterials. *Environ. Sci. Technol.* **2006**, *40* (14), 4336−4345.

(9) Yuan, S.-J.; Chen, J.-J.; Lin, Z.-Q.; Li, W.-W.; Sheng, G.-P.; Yu, H.-Q. Nitrate formation from atmospheric nitrogen and oxygen photocatalysed by nano-sized titanium dioxide. *Nat. Commun.* **2013**, *4*, 1−7.

(10) Nebbioso, A.; Piccolo, A. Molecular characterization of dissolved organic matter (DOM): A critical review. *Anal. Bioanal. Chem.* **2013**, *405* (1), 109−124.

(11) Valencia, S.; Marín, J. M.; Restrepo, G.; Frimmel, F. H. Evaluation of natural organic matter changes from Lake Hohloh by three-dimensional excitation−emission matrix fluorescence spectroscopy during TiO_2/UV process. *Water Res.* **2014**, *51* (0), 124−133.

(12) Loosli, F.; Le Coustumer, P.; Stoll, S. Effect of natural organic matter on the disagglomeration of manufactured TiO_2 nanoparticles. *Environ. Sci.: Nano* **2014**, *1*, 154−160.

(13) Gallego-Urrea, J. A.; Perez Holmberg, J.; Hassellov, M. Influence of different types of natural organic matter on titania nanoparticle stability: Effects of counter ion concentration and pH. *Environ. Sci.: Nano* **2014**, *1*, 181−189.

(14) Loosli, F.; Le Coustumer, P.; Stoll, S. TiO_2 nanoparticles aggregation and disaggregation in presence of alginate and Suwannee River humic acids. pH and concentration effects on nanoparticle stability. *Water Res.* **2013**, *47* (16), 6052−6063.

(15) Yan, M.; Li, M.; Wang, D.; Xiao, F. Optical property of iron binding to Suwannee River fulvic acid. *Chemosphere* **2013**, *91* (7), 1042−1048.

(16) Chen, W. B.; Smith, D. S.; Guéguen, C. Influence of water chemistry and dissolved organic matter (DOM) molecular size on copper and mercury binding determined by multiresponse fluorescence quenching. *Chemosphere* **2013**, *92* (4), 351−359.

(17) Lu, X.; Jaffe, R. Interaction between Hg(II) and natural dissolved organic matter: A fluorescence spectroscopy based study. *Water Res.* **2001**, *35* (7), 1793−1803.

(18) Ishii, S. K. L.; Boyer, T. H. Behavior of reoccurring PARAFAC components in fluorescent dissolved organic matter in natural and engineered systems: A critical review. *Environ. Sci. Technol.* **2012**, *46* (4), 2006−2017.

(19) Wu, F. C.; Mills, R. B.; Evans, R. D.; Dillon, P. J. Kinetics of metal−fulvic acid complexation using a stopped-flow technique and three-dimensional excitation emission fluorescence spectrophotometer. *Anal. Chem.* **2003**, *76* (1), 110−113.

(20) Lumsdon, D. G.; Fraser, A. R. Infrared spectroscopic evidence supporting heterogeneous site binding models for humic substances. *Environ. Sci. Technol.* **2005**, *39* (17), 6624−6631.

(21) Chen, J.; Gu, B.; LeBoeuf, E. J.; Pan, H.; Dai, S. Spectroscopic characterization of the structural and functional properties of natural organic matter fractions. *Chemosphere* **2002**, *48* (1), 59−68.

(22) Noda, I. Close-up view on the inner workings of two-dimensional correlation spectroscopy. *Vib. Spectrosc.* **2012**, *60* (0), 146−153.

(23) Yu, G.-H.; Tang, Z.; Xu, Y.-C.; Shen, Q.-R. Multiple fluorescence labeling and two dimensional FTIR−^{13}C NMR heterospectral correlation spectroscopy to characterize extracellular polymeric substances in biofilms produced during composting. *Environ. Sci. Technol.* **2011**, *45* (21), 9224−9231.

(24) Noda, I.; Ozaki, Y. *Two-Dimensional Correlation Spectroscopy - Applications in Vibrational and Optical Spectroscopy*; John Wiley & Sons Ltd: London, 2004.

(25) Abdulla, H. A. N.; Minor, E. C.; Hatcher, P. G. Using two-dimensional correlations of ^{13}C NMR and FTIR to investigate changes in the chemical composition of dissolved organic matter along an estuarine transect. *Environ. Sci. Technol.* **2010**, *44* (21), 8044−8049.

(26) Yan, W.; Zhang, J.; Jing, C. Adsorption of Enrofloxacin on montmorillonite: Two-dimensional correlation ATR/FTIR spectroscopy study. *J. Colloid Interface Sci.* **2013**, *390* (1), 196−203.

(27) Yu, G.-H.; Wu, M.-J.; Wei, G.-R.; Luo, Y.-H.; Ran, W.; Wang, B.-R.; Zhang, J. c.; Shen, Q.-R. Binding of organic ligands with Al(III) in dissolved organic matter from soil: Implications for soil organic carbon storage. *Environ. Sci. Technol.* **2012**, *46* (11), 6102−6109.

(28) Xu, H.; Yu, G.; Yang, L.; Jiang, H. Combination of two-dimensional correlation spectroscopy and parallel factor analysis to characterize the binding of heavy metals with DOM in lake sediments. *J. Hazard. Mater.* **2013**, *263* (Part 2, (0)), 412−421.

(29) Stevenson, F. J. *Humus Chemistry: Genesis, Composition, Reactions*; John Wiley & Sons, Inc.: New York, 1994.

(30) Li, W.-H.; Sheng, G.-P.; Lu, R.; Yu, H.-Q.; Li, Y.-Y.; Harada, H. Fluorescence spectral characteristics of the supernatants from an anaerobic hydrogen-producing bioreactor. *Appl. Microbiol. Biotechnol.* **2011**, *89* (1), 217−224.

(31) Lu, R.; Sheng, G.; Li, W.; Yu, H.; Raichlin, Y.; Katzir, A.; Mizaikoff, B. IR-ATR Chemical Sensors Based on Planar Silver Halide Waveguides Coated with an Ethylene/Propylene Copolymer for Detection of Multiple Organic Contaminants in Water. *Angew. Chem., Int. Ed.* **2013**, *52* (8), 2265−2268.

(32) Domínguez-Vidal, A.; Saenz-Navajas, M. P.; Ayora-Cañada, M. J.; Lendl, B. Detection of albumin unfolding preceding proteolysis using fourier transform infrared spectroscopy and chemometric data analysis. *Anal. Chem.* **2006**, *78* (10), 3257−3264.
(33) Jia, Q.; Wang, N.-N.; Yu, Z.-W. An insight into sequential order in two-dimensional correlation spectroscopy. *Appl. Spectrosc.* **2009**, *63* (3), 344−353.
(34) Yan, M.; Fu, Q.; Li, D.; Gao, G.; Wang, D. Study of the pH influence on the optical properties of dissolved organic matter using fluorescence excitation−emission matrix and parallel factor analysis. *J. Lumin.* **2013**, *142* (0), 103−109.
(35) Yamashita, Y.; Jaffé, R. Characterizing the interactions between trace metals and dissolved organic matter using excitation−emission matrix and parallel factor analysis. *Environ. Sci. Technol.* **2008**, *42* (19), 7374−7379.
(36) Avena, M. J.; Wilkinson, K. J. Disaggregation kinetics of a peat humic acid: Mechanism and pH effects. *Environ. Sci. Technol.* **2002**, *36* (23), 5100−5105.
(37) Brigante, M.; Zanini, G.; Avena, M. On the dissolution kinetics of humic acid particles - Effects of pH, temperature and Ca^{2+} concentration. *Colloids Surf., A* **2007**, *294* (1−3), 64−70.